Original Article

DOI: 10.5582/bst.2026.01000

PRXL2B facilitates the progression of hepatocellular carcinoma and the therapeutic efficacy of oncolytic adenovirus H101 through the PI3K/AKT/PD-L1 axis

Ziqi Zhang[1,§], Hongli Chen[2,§], Yangming Liu[3,§], Hao Wang[1], You Yan[1,4], Yanxi Yu[1], Zuotian Huang[1], Yanyao Liu[1], Wei Li[1], Zhongjun Wu[1], Meiqing Kang[1], Xiaoyong Luo[5], Ping Che[6,*], Rui Liao[1,*]

[1] Department of Hepatobiliary Surgery, The First Affiliated Hospital of Chongqing Medical University, Chongqing, China;
[2] Nanchuan District Maternal and Child Health Care Hospital, Chongqing, China;
[3] Department of Obstetric, The Affiliated Banan Hospital of Chongqing Medical University, Chongqing, China;
[4] Department of Pathology, The Second Affiliated Hospital of Chongqing Medical University, Chongqing, China;
[5] Department of Gastrointestinal Surgery, Chongqing Jiulongpo People's Hospital, Chongqing, China;
[6] Department of Hepatobiliary Surgery, Shapingba Hospital affiliated to Chongqing University (Shapingba District People's Hospital of Chongqing), Chongqing, China.

SUMMARY: Oncolytic adenovirus H101 has shown antitumor activity in hepatocellular carcinoma (HCC), but the molecular determinants of treatment response remain unclear. In this study, a Hepa1-6 subcutaneous tumor model was established in C57BL/6 mice and treated with intratumoral H101, followed by integrated transcriptomic and proteomic analyses to identify candidate genes associated with H101 response. PRXL2B was selected for further investigation using public multi-omics datasets, tissue microarray-based immunohistochemistry, *in vitro* functional assays, mechanistic analyses, and *in vivo* validation experiments. Integrated multi-omics analyses identified PRXL2B as a candidate gene downregulated after H101 treatment. Public datasets and tissue-based validation further showed that PRXL2B was upregulated in HCC tissues. In MHCC97H and HCCLM3 cells, PRXL2B knockdown inhibited proliferation, migration, and invasion, promoted apoptosis and cell-cycle arrest, and enhanced the antitumor effect of H101. Mechanistically, PRXL2B silencing reduced AKT phosphorylation and PD-L1 expression. *In vivo*, PRXL2B knockdown suppressed tumor growth, and the combination of PRXL2B knockdown and H101 produced the strongest antitumor effect. These findings indicate that PRXL2B promotes malignant phenotypes in HCC and may modulate H101 efficacy through the PI3K/AKT/PD-L1 axis. Targeting PRXL2B may therefore represent a potential strategy to enhance the therapeutic efficacy of oncolytic virus therapy in HCC.

Keywords: hepatocellular carcinoma, oncolytic adenovirus, H101, PRXL2B, PD-L1

1. Introduction

Hepatocellular carcinoma (HCC), as the most prevalent subtype of primary liver cancer, persists as a primary cause of cancer-related mortality globally. Curative treatments, such as resection, local ablative procedures, and transplantation, can improve survival rates among carefully selected early-stage patients (*1*). Nevertheless, due to the asymptomatic progression and delayed detection, a substantial number of patients are diagnosed with advanced-stage disease, precluding the application of potentially curative therapies. For these patients, targeted therapy and immune checkpoint inhibitors (ICIs) have the potential to enhance overall survival. However, their efficacy is still constrained by tumor heterogeneity, immune microenvironment suppression, and acquired resistance (*2*). Consequently, exploring novel strategies that integrate "direct tumor cell killing" with "immune remodeling" remains a critical direction for HCC treatment.

Oncolytic virus (OV) therapy exerts its effects *via* dual mechanisms. Firstly, it selectively replicates within tumor cells and causes their lysis (*3*). Secondly, it induces immunogenic cell death, facilitates the release of tumor antigens, and activates both innate and adaptive immune responses (*4*). This therapeutic approach has gained increasing attention since the early studies in the 1950s, where the first viral agents were used in cancer treatment, and has since evolved with the development of genetically modified oncolytic viruses that can

selectively target cancer cells. H101, a recombinant adenoviral oncolytic agent, has demonstrated clinical potential in several tumor types, such as non-small cell lung cancer, head and neck squamous cell carcinoma, glioblastoma, and HCC (*5-7*). In particular, its use in HCC has shown promise in preclinical and clinical trials, offering a new strategy to target both tumor cells and the immune microenvironment (*8*). Nevertheless, the efficacy of OV varies significantly across different tumor types and among individuals. This variability is partly due to differences in the tumor microenvironment and the immune system's ability to recognize and respond to the viral infection (*9*). The key molecules and predictive biomarkers related to its response remain unclear. Recent studies suggest that immune checkpoint proteins, such as PD-L1, and tumor-intrinsic factors, like mutations in the PI3K/AKT pathway, may influence OV therapy efficacy in HCC (*10*). In particular, the tumor-intrinsic factors and downstream immune regulation mechanisms that influence the sensitivity and tolerance of oncolytic adenovirus therapy in HCC require further clarification (*11*).

Multi-omics investigations, encompassing transcriptomics and proteomics, have emerged as potent methodologies to characterize alterations in tumor molecular profiles subsequent to therapeutic interventions. These studies contribute to surmounting the limitations of single-omics approaches, which frequently encounter discrepancies between transcriptional and protein-level data. Through the integration of transcriptomic and proteomic data, more robust candidate molecules can be identified, thereby furnishing a more reliable foundation for comprehending molecular mechanisms and translating research findings into clinical applications (*12*). In recent years, multi-omics has been applied in HCC research to uncover novel therapeutic targets and biomarkers. For instance, studies have amalgamated genomic, transcriptomic, and proteomic data to identify pivotal signaling pathways implicated in HCC progression. A study demonstrated that the integration of proteomic and transcriptomic profiles could assist in identifying potential therapeutic targets such as PD-L1 and VEGF in HCC, offering insights into immune evasion mechanisms and tumor vascularization (*13*). Furthermore, a study in employed multi-omics approaches to analyze alterations in the tumor microenvironment (TME) in HCC, revealing novel perspectives on how metabolic shifts in the TME influence tumorigenesis. By integrating metabolomics with transcriptomics and proteomics, the researchers were able to uncover novel biomarkers associated with a poor prognosis in HCC patients (*14*). This approach underscored the crucial role of metabolic reprogramming in the development and progression of liver cancer. Another study in utilized multi-omics to explore the role of long non-coding RNAs (lncRNAs) in HCC, integrating RNA sequencing, proteomics, and epigenomics to delineate lncRNA-associated pathways in HCC. The integration of these data provided a more in-depth understanding of epigenetic regulation in liver cancer progression, presenting potential lncRNA targets for therapeutic intervention (*15*). These examples illustrate the substantial potential of multi-omics in understanding HCC biology and in the development of personalized medicine strategies for liver cancer (*16*).

In the present study, an immunocompetent Hepa1-6 subcutaneous tumor model was employed to assess the effects of intratumoral H101 treatment. Transcriptomic and proteomic data were integrated to identify response-related genes, and PRXL2B was selected as a key target. The findings were further validated using multi-omics data, immunohistochemistry of HCC tissue microarrays, *in vitro* functional assays, and mechanistic studies (PI3K/AKT-PD-L1 axis), along with *in vivo* combination therapy experiments, to clarify the role of PRXL2B in HCC progression and the efficacy of H101.

2. Materials and Methods

2.1. Cells and culture

Mouse Hepa1-6 cells, Hepatic progenitor cells (derived from mouse liver), Telomerase-immortalized human liver epithelial cells, Human hepatocellular carcinoma cells, and human liver cancer cell lines MHCC97H and HCCLM3 were purchased from Sevier (China). Animal experiments were approved by the Ethics Committee of Chongqing Medical University (IACUC-CQMU-2024-11061). Cells were cultured in DMEM supplemented with 10% fetal bovine serum (FBS, Procell) and 1% penicillin-streptomycin at 37°C in a 5% CO_2 incubator. Cells were passaged at a ratio of 1:3 to 1:5 and used for experiments during the logarithmic growth phase. H101 was purchased from Ankerui. *In vitro* infection was performed at a multiplicity of infection (MOI) of 0.05 for 96 hours, as previously described in Song *et al*., 2025 (*17*). The experimental groups were NC, shPRXL2B, and shPRXL2B + H101.

2.2. Clinical sample collection

The animal experiments were approved by the Ethics Committee of Chongqing Medical University (Approval No: IACUC-CQMU-2024-11061). The tissue microarray study was approved by the Ethics Committee of the First Affiliated Hospital of Chongqing Medical University (Approval No: 2024-607-01). A total of 84 pathological paraffin-embedded samples (including 84 HCC samples and 83 adjacent normal liver tissue samples) were collected from patients who underwent surgery at Chongqing Medical University between 2020 and 2023. Survival data from 84 patients who participated in postoperative follow-up were also included. These samples were used for tissue microarray preparation and

subsequent immunohistochemistry (IHC) and in situ hybridization analysis. All participants provided written informed consent. The samples were pathologically confirmed as HCC after surgery. All studies were conducted in accordance with the principles of the Declaration of Helsinki and the Istanbul Declaration.

2.3. Subcutaneous tumor implantation and treatment

Female C57BL/6 mice (7–8 weeks old) were used to establish subcutaneous Hepa1-6 tumor models. The mice were inoculated subcutaneously with 2×10^6 Hepa1-6 cells in PBS. When the tumor volume reached approximately 80 mm^3, intratumoral injections of H101 (1×10^8 PFU per dose, diluted in PBS, 80–120 μL per dose) were administered daily for 3 consecutive days, starting on day 9. The tumors were harvested on day 14. The tumor volume was calculated using the formula $V = 0.5 \times \text{length} \times \text{width}^2$. The experiment included 4 mice per group. All animal experiments were approved by the Ethics Committee of Chongqing Medical University (IACUC-CQMU-2024-11061).

2.4. Virus/plasmid construction and PRXL2B knockdown

PRXL2B expression was knocked down using shRNA. Human-shRNA-1 (h-sh1) and mouse-shRNA-1 (m-sh1) were used for *in vitro* and *in vivo* experiments, respectively. The shRNA vector was pLVX-shRNA2-Puro (BamHI/EcoRI cloning). The sequences are as follows (suggested for inclusion in the supplementary materials):

h-shPRXL2B-1 (insert sequence):
GATCGGGATGAGAGCAAGCAGCTTTACTCGAGT
AAAGCTGCTTGCTCTCATCCTTTTTT
M-shPRXL2B-1 (insert sequence):
GATCGATGAGAGCAAGCAAATCTATACTCGAGTA
TAGATTTGCTTGCTCTCATTTTTTT

Stable cell lines were selected using puromycin. Sensitivity for shRNA screening was optimized by titrating concentrations in pilot experiments, typically ranging from 1–3 μg/mL for 3–5 days.

2.5. Transcriptomics, proteomics analysis and multi-omics integration

Total RNA was extracted from tumor tissues using TRIzol reagent (Thermo Fisher Scientific, USA). cDNA libraries were constructed using SuperScript™ II Reverse Transcriptase (Invitrogen, USA). Paired-end sequencing (2 × 150 bp) was carried out using the Illumina NovaSeq™ 6000 platform. Differentially expressed genes (DEGs) were identified using DESeq2 with thresholds of $|\log2 \text{ - fold change}| \geq 1$ and FDR < 0.05. GO and KEGG enrichment analyses were conducted on DEGs. For proteomics, the raw data were processed using the Thermo Orbitrap Fusion Lumos platform and analyzed using Proteome Discoverer. Protein quantification was normalized using row means and column medians. Differential protein analysis was conducted with a p-value < 0.05 and FC > 1.2 or FC < 0.83. Pathway enrichment was carried out using standard enrichment factor calculations and presented as bubble plots. We integrated transcriptomic DEGs and proteomic differential proteins to identify robust candidate genes. Directionally consistent genes were selected for further validation based on their biological significance.

2.6. Immunohistochemistry and scoring

Immunohistochemical analysis was performed on a tissue microarray (TMA) cohort of 84 HCC samples to assess PRXL2B expression. This tissue microarray study was approved by the Ethics Committee of the First Affiliated Hospital of Chongqing Medical University (Approval No: 2024-607-01). The antibody used for PRXL2B detection was the C1orf93 polyclonal antibody (Proteintech, Catalog No: 26304-1-AP, Rabbit, IgG isotype), which was applied at the recommended dilution of 1:600. The H-score was calculated based on the staining intensity and the percentage of positive cells, classifying PRXL2B expression into high and low groups for subsequent survival analysis. The immunohistochemical procedure involved deparaffinization and rehydration of tissue sections, followed by antigen retrieval. The sections were incubated with the primary antibody (C1orf93, diluted 1:600) at room temperature for 1.5 hours. After incubation, the sections were washed and treated with a secondary antibody, followed by appropriate substrate development for visualization. The stained tissue sections were then evaluated by two independent pathologists to determine the staining intensity and the percentage of positively stained cells.

2.7. Western blot and antibodies

Cells were lysed in RIPA lysis buffer (Beyotime, China) for 10 minutes at 4°C. The supernatant was collected and centrifuged at 15,000 rpm for 15 minutes at 4°C. Protein concentration was measured using the BCA protein assay kit (Solarbio, Beijing, China). A total of 20 μg of protein was boiled and separated by 12.5% SDS-PAGE, then transferred to a PVDF membrane (Millipore, USA). The membrane was blocked with 5% non-fat milk for 1 hour, followed by incubation with primary antibodies at 4°C: PRXL2B (1:500, Proteintech #26304-1-AP, China), AKT (1:5000, Proteintech 10176-2-AP, China), p-AKT (1:2000; Proteintech #66444-1-Ig, China), PD-L1 (1:2000; 66248-1-Ig, Proteintech, China), and GAPDH (1:2000; #60004-1-Ig, Proteintech, China). Protease/phosphatase inhibitor cocktail (Beyotime, Catalog No. P1081, 50X) was added during the protein

extraction process to prevent protein degradation and dephosphorylation.

2.8. Cell migration and invasion assays

A wound healing assay was conducted to evaluate cell migration. Cells (5×10^6 cells per well) were seeded in 6-well plates. Once the cells reached 100% confluence, a 200 μl pipette tip was employed to create a scratch in the cell monolayer. The wounds were infected with H101 at a multiplicity of infection (MOI) of 0.05. Wound healing was monitored at designated intervals over 48 hours. Images were captured from five distinct angles per well and analyzed using ImageJ software (version 1.52) to measure the wound area. The percentage of wound healing was quantified using the following formula: [1-(Wound Area at Tt/Wound Area at T0)]×100%. Transwell assays were used to evaluate cell migration and invasion. For the migration assay, 10^4 cells were plated in 100 μl of serum-free medium in 24-well inserts (Corning, USA). For the invasion assay, cells were plated on Matrigel-coated inserts (Beyotime, China). To each insert, 100 μL of medium with H101 (MOI = 0.05) or serum-free medium was added. In the lower chamber, 500 μL of medium with 10% FBS was used as a chemoattractant. After 24 hours of incubation, non-migrating or non-invading cells in the upper chamber were removed using a cotton swab. Cells that had migrated or invaded through the insert were fixed with 4% paraformaldehyde and stained with 0.1% crystal violet. The number of migrating or invading cells in three random fields was quantified under an inverted microscope (Leica, Germany).

2.9. Cell apoptosis detection

Cells were harvested from one well of a 6-well plate. Floating cells were collected in a centrifuge tube, and adherent cells were digested with 0.25% trypsin to obtain single cells, ensuring not to over-digest. The cells were washed twice with PBS at 1000 rpm for 5 minutes. Cells (1×10^6) were resuspended in 500 μL of PBS (PH = 7.2) and stored in 1.5 mL EP tubes for apoptosis detection.

2.10. Cell cycle detection

Cells were harvested from one well of a 6-well plate. Floating cells were collected in a centrifuge tube. The adherent cells were digested with 0.25% trypsin to obtain single cells, again ensuring to avoid over-digestion. The cells were washed twice with PBS at 1000 rpm for 5 minutes and resuspended in 100 μL of PBS. Slowly, 900 μL of pre-chilled 75% ethanol was added while gently shaking to prevent cell aggregation. The cells were stored at 4°C for 2-3 weeks. Flow cytometry analysis of cell cycle and apoptosis was performed using a Attune NxT flow cytometer (Thermo Fisher Scientific, USA), and data were analyzed using Modfit software (version 4.1).

2.11. Cell proliferation assay

According to the manufacturer's instructions, the Cell Count Kit-8 (CCK-8) (Topscience, China) was used to conduct cell proliferation assays. 1×10^4 HCC97-H and HCC-LM3 cells were seeded in 96-well plates and infected with the virus as described in the virus growth assays. At various time points (0, 24, 48, 72, and 96 hours), 10 μL of CCK-8 solution (mixed with 100 μL DMEM medium) was added to each well and incubated at 37°C for 1 hour. The optical density (OD) was measured using a microplate reader (Bio-Rad, USA) at 450 nm.

2.12. Statistical analysis

Statistical comparisons were conducted using Student's *t*-test for two-group Statistical comparisons were conducted using Student's *t*-test for two-group comparisons (with normality tested). One-way ANOVA with post-hoc testing was employed for multiple group comparisons. Survival analysis was carried out using Kaplan-Meier curves and log-rank tests. Cox regression analysis was performed for both univariate and multivariate models. Statistical analyses were performed using GraphPad Prism version 9.0 (GraphPad Software, USA) for *t*-test and ANOVA, and SPSS version 26.0 (IBM, USA) for Kaplan–Meier survival analysis and Cox regression.

3. Results

3.1. H101 inhibition of tumor growth and identification of response-related genes

To assess the impact of oncolytic adenovirus H101 on liver cancer growth, a subcutaneous Hepa1-6 tumor model was established in immunocompetent female C57BL/6 mice. When the tumor volume approximated 80 mm^3, H101 (1×10^8 PFU per dose, diluted in PBS) was administered *via* intratumoral injection once daily for three consecutive days, commencing on day 9. Tumors were excised on day 14 for subsequent omics analysis (n = 4 per group) (Figure 1a). In comparison with the control group, the tumors in the H101-treated group exhibited a substantial reduction in size at the experimental endpoint (Figure 1b). Tumor growth curves demonstrated that H101 treatment significantly impeded tumor volume expansion (Figure 1c), and the tumor weight at the endpoint was also significantly decreased (Figure 1d, two-tailed Student's *t*-test, p = 0.027). To analyze the molecular characteristics of the tumors subsequent to H101 treatment, RNA-seq and proteomics analyses were conducted on tumor tissues (log2FC of Transcriptomic = -0.9300, P-value of Transcriptomic

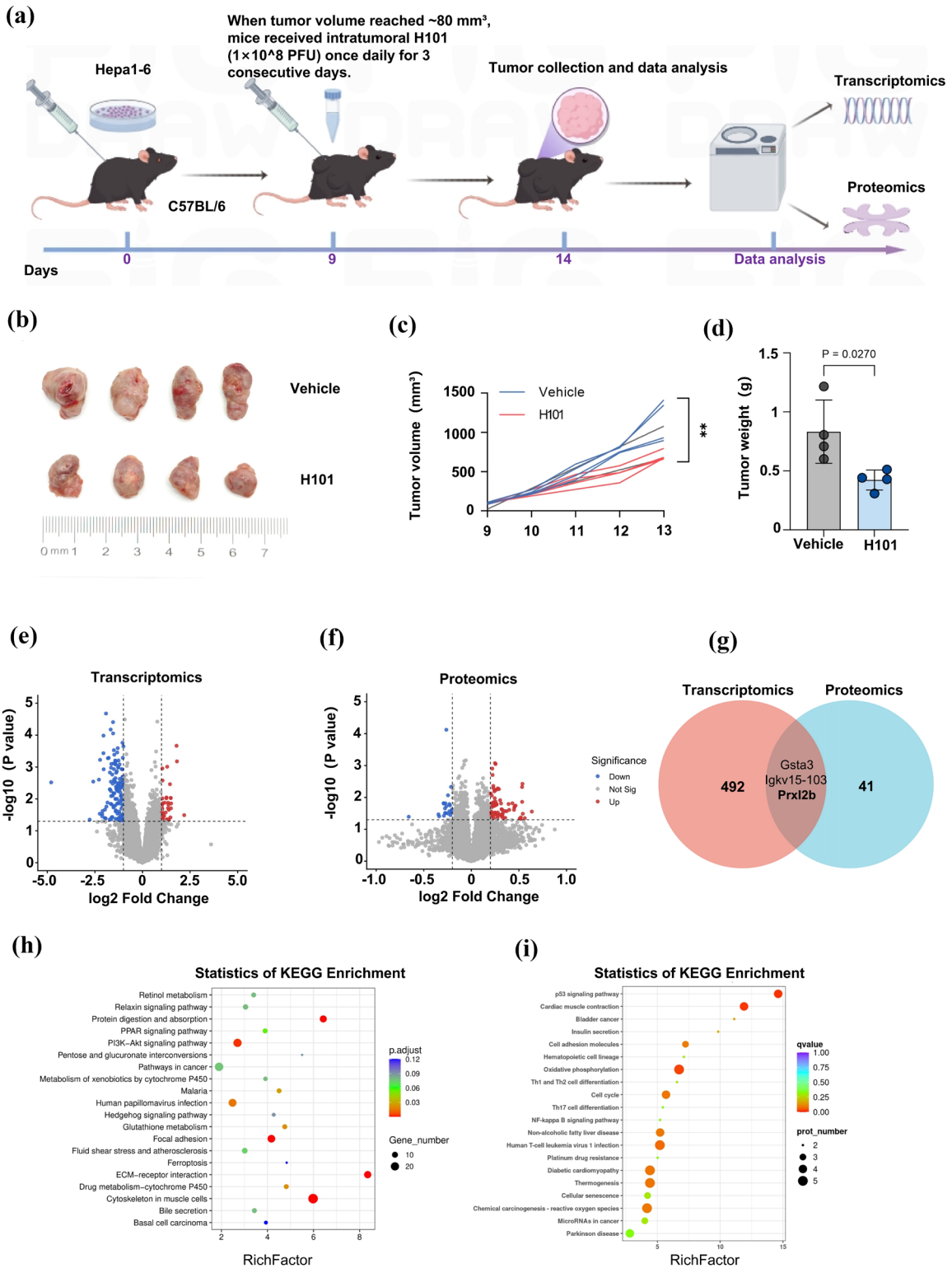

Figure 1. Intratumoral H101 suppresses Hepa1-6 subcutaneous tumor growth and identifies PRXL2B through integrated transcriptomic and proteomic analyses. (a) Schematic illustration of the experimental design. Female C57BL/6 mice were subcutaneously inoculated with Hepa1-6 cells (2×10^6). When tumors reached approximately 80 mm^3, mice received intratumoral H101 injections (1×10^8 PFU) once daily for 3 consecutive days beginning on day 9. Tumors were collected on day 14 for transcriptomic and proteomic analyses ($n = 4$ per group). **(b)** Representative images of excised tumors collected at day 14. **(c)** Tumor growth curves. Tumor volume was calculated as V = 0.5 × length × $width^2$. **(d)** Tumor weights at day 14. Data are presented as mean ± SD with individual values. Statistical significance was determined using a two-tailed Student's *t*-test. **(e)** Volcano plot of differentially expressed genes (DEGs) identified by RNA-seq analysis in H101-treated and PBS-treated tumors. **(f)** Volcano plot of differentially expressed proteins identified by proteomic analysis in H101-treated and PBS-treated tumors. **(g)** Venn diagram showing the overlap between transcriptomic and proteomic analyses, with PRXL2B highlighted. **(h)** KEGG pathway enrichment analysis of transcriptomic DEGs **(h)** and differentially expressed proteins **(i)** The x-axis indicates the enrichment factor (GeneRatio). Dot size represents gene/protein counts, and dot color indicates adjusted P values.

= 0.0200 and log2FC of Proteomic = -1.5327, *p*-value of Proteomic = 0.0038). Volcano plots revealed a considerable number of differentially expressed genes (DEGs), with two genes being upregulated and one gene being downregulated (Figure 1e). Significant differential proteins were also detected through proteomics analysis (Figure 1f). Further integration of RNA-seq DEGs with differential proteins from proteomics yielded three common candidate molecules (Figure 1g), suggesting that these molecules could serve as stable core nodes involved in the H101 response. Pathway enrichment analysis indicated that the differential molecules were predominantly enriched in tumor-associated signaling pathways, with the PI3K/AKT pathway being one of the significantly enriched pathways (Figure 1h–i). This implies that the antitumor effects of H101 may be regulated by this classical oncogenic pathway. Based on the expression direction and potential biological significance of the intersecting candidate molecules, PRXL2B (C1orf93), which was downregulated following H101 treatment, was selected as the key target for further investigation. Integrated transcriptomic and proteomic analyses identified PRXL2B as a candidate gene associated with H101 treatment. Because PRXL2B was consistently downregulated after H101 treatment and showed potential biological relevance, it was selected for further investigation.To further explore the role of PI3K/AKT pathway in HCC progression, Gene Set Enrichment Analysis (GSEA) was conducted on the transcriptomic and proteomic data. The PI3K/AKT pathway was significantly enriched, with high NES values and low P-values, indicating its important role in tumor progression and potential modulation by H101 therapy (Supplementary Figure S1, *https://www.biosciencetrends.com/action/getSupplementalData.php?ID=303*).

3.2. Multi-omics analysis reveals PRXL2B upregulation in HCC and its correlation with prognosis and PI3K/AKT pathway activity

To explore the expression pattern and potential clinical implications of PRXL2B in HCC, we initially analyzed data from the TCGA database. Pan-cancer analysis indicated that PRXL2B exhibited abnormal expression across diverse cancer types, and a notable differential expression was detected in the hepatocellular carcinoma (LIHC/HCC) cohort (Figure 2a). In independent GEO datasets (GSE54236, GSE144269), the expression of PRXL2B was consistently elevated in HCC tissues compared to non-tumor tissues (Figure 2b), suggesting that PRXL2B may exert a promotional effect on HCC development. We further assessed the relationship between PRXL2B expression and disease progression, as well as the activity of the PI3K/AKT pathway. Stage-associated analysis revealed disparities in PRXL2B expression among different clinical stages (Figure 2c). Moreover, PRXL2B expression was significantly correlated with the PI3K/AKT pathway activity score (Figure 2c), which was in line with the observed enrichment of the PI3K/AKT pathway in tumor omics analysis. Kaplan–Meier survival analysis demonstrated a significant association between PRXL2B expression and overall survival (OS), disease-specific survival (DSS), progression-free interval (PFI), and disease-free interval (DFI) (Figure 2d). Spatial transcriptomics data further indicated that PRXL2B signals were predominantly localized in tumor regions rather than non-malignant regions (Figure 2e-f), corroborating its expression profile associated with tumor cells.

3.3. Clinical validation of PRXL2B upregulation and its prognostic significance in HCC

To validate the expression of PRXL2B in clinical HCC samples, an IHC analysis was conducted on a TMA cohort comprising 84 paired tumor and adjacent non-tumor tissue samples. The relationship between PRXL2B expression and clinicopathologic features in 84 HCC patients is presented in Table 1. The H-score of PRXL2B was correlated with various clinical characteristics, including age, gender, HBsAg status, AFP level, vascular invasion, tumor size, differentiation, and stage (Figure 3a).The expression of PRXL2B was high in tumor tissues, as evidenced by representative IHC images (Figure 3b).The correlation between PRXL2B expression and clinicopathological features was also analyzed. In the clinical cohort, PRXL2B expression was associated with overall survival; however, the statistical significance of this correlation may vary depending on the selected cutoff and follow-up duration (Figure 3c). When compared with paired adjacent tissues, the H-scores of PRXL2B were significantly higher in tumor tissues (Figure 3d), indicating an upregulation of PRXL2B in HCC tissues. Additionally, Western blotting of paired tumor and adjacent tissue samples corroborated the upregulation of PRXL2B protein expression in tumors (Figure 3e). These clinical findings, in conjunction with bioinformatics analysis, suggest that PRXL2B is upregulated in HCC and may be associated with disease progression and prognosis.

3.4. PRXL2B knockdown inhibits malignant phenotypes and enhances H101 efficacy *in vitro*

To investigate the functional role of PRXL2B in HCC cells, the protein expression of PRXL2B was initially quantified in various liver cancer cell lines. Differential expression of PRXL2B was detected among the HCC cell lines (Figure 4a). MHCC97H and HCCLM3 cells were chosen for subsequent functional studies. After establishing PRXL2B knockdown models, the cells were divided into the negative control (NC), shPRXL2B, and shPRXL2B + H101 groups. The cells in these groups were infected with H101 at a multiplicity of infection

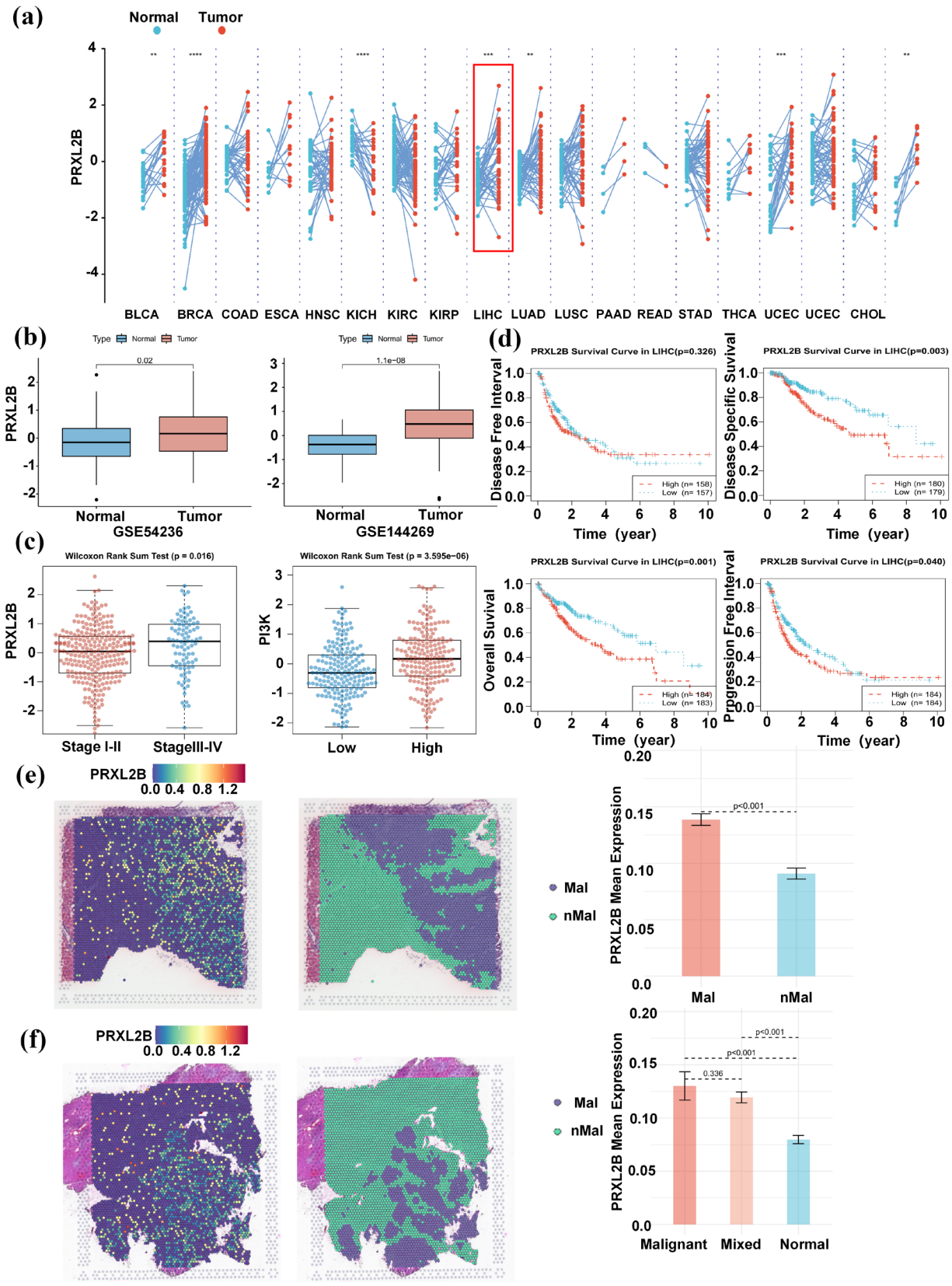

Figure 2. Multi-omics analyses support PRXL2B upregulation in HCC and its association with prognosis and PI3K/AKT pathway activity. **(a)** Pan-cancer analysis of PRXL2B expression in tumor and normal tissues, with the LIHC cohort highlighted. **(b)** Differential expression analysis of PRXL2B in HCC and non-tumor tissues across multiple GEO datasets. **(c)** Correlation analysis of PRXL2B expression with clinical stage and PI3K/AKT pathway activity. **(d)** Kaplan–Meier survival analysis of PRXL2B expression in the TCGA-LIHC cohort. **(e–f)** Spatial transcriptomic analysis of PRXL2B expression, including spatial distribution patterns and comparisons between different tissue regions/groups.

Table 1. The relationship of PRXL2B expression with clinicopathologic features in 84 HCC patients

Variables	Number of patients		
	PRXL2B low expression	PRXL2B high expression	*p*
Gender			ns
Mele	38	28	
Female	8	9	
Age (Years)			ns
> 60	9	12	
≦ 60	37	25	
Differentiatation			0.029
Well/moderate	33	25	
poor	12	12	
AFP			0.035
≧ 25	11	9	
< 25	34	28	
Vascular Invasion			0.040
MVI (+)	18	14	
MVI (-)	27	23	
HBsAg			ns
Positive	41	31	
Negative	4	6	
Cirrhosis			ns
yes	29	29	
no	16	8	
Tumor size (cm)			0.032
≧ 5	9	9	
< 5	36	28	
BCLC stage			0.025
0/A	35	35	
B/C/D	10	2	

(MOI) of 0.05 for 96 hours. CCK-8 assays indicated that the knockdown of PRXL2B significantly diminished cell viability in both MHCC97H and HCCLM3 cells, and the combined treatment with H101 further augmented this inhibitory effect (Figure 4b–c). Transwell migration and invasion assays additionally demonstrated that the knockdown of PRXL2B significantly curtailed cell migration and invasion in both cell lines (Figure 4d,f). Wound healing assays presented consistent findings (Figure 4e,g). Regarding mechanistic phenotypes, flow cytometry revealed that the knockdown of PRXL2B elevated the apoptosis rate (Figure 4h) and modified cell cycle distribution, with G2 - phase arrest being observed in HCCLM3 cells (Figure 4i). These *in vitro* results illustrate that the knockdown of PRXL2B significantly suppresses the malignant phenotypes of HCC cells and potentiates the antitumor effects of H101.

3.5. PRXL2B regulates AKT phosphorylation and PD-L1 expression, enhancing *in vivo* antitumor efficacy

To further clarify the molecular mechanisms underpinning PRXL2B knockdown, RNA-seq analysis was performed on MHCC97H cells (biological replicates3) under normal control (NC) and short hairpin RNA targeting PRXL2B (shPRXL2B) conditions. Differential analysis and volcano plots indicated the presence of significant differentially expressed genes (DEGs) subsequent to PRXL2B knockdown (Figure 5a). Enrichment analysis demonstrated that these DEGs were significantly enriched in immune-related and tumor signaling pathways (Figure 5b-c), and the programmed death-ligand 1 (PD-L1) axis, which participates in immune evasion, was identified as a potential target. In light of the observed enrichment of the PI3K/AKT pathway in our murine tumor data, we conducted further investigations into the phosphorylation status of AKT and the expression of PD-L1. Western blot analysis demonstrated that knockdown of PRXL2B led to a substantial reduction in p-AKT levels and down-regulated PD-L1 expression, as compared with the negative control (NC) group. The combined treatment with H101 further augmented these effects (Figure 5d). Densitometric quantification verified the consistent decline in PD-L1 (normalized to GAPDH), PRXL2B (normalized to GAPDH and expressed relative to NC), and the p-AKT/AKT ratio (relative to NC) (Figure 5e–g). These findings suggest that PRXL2B modulates the PI3K/AKT pathway and PD-L1 expression, which is associated with immune evasion and influences the response to H101 treatment. Finally, the *in-vivo* antitumor effects of PRXL2B knockdown in combination with H101 were validated within the Hepa1-6 subcutaneous tumor model. In comparison to the NC group, the growth rate of tumors in the shPRXL2B group was notably slower. Furthermore, the combination of PRXL2B knockdown and H101 resulted in the most substantial reduction in tumor volume and weight at the experimental endpoint (Figure 5h–j). These *in-vivo* results, when integrated with the *in-vitro* findings, imply that PRXL2B plays a pivotal role in regulating the malignancy of HCC, and its inhibition may augment the efficacy of oncolytic virus therapy. To further validate the involvement of the PI3K/AKT pathway and immune evasion *in vivo*, immunohistochemical (IHC) staining was performed on tumor tissues. As shown in Figure 5k, the expression levels of p-AKT and PD-L1 were significantly decreased in the shPRXL2B group compared with the NC group. Quantitative analysis confirmed a consistent reduction in both markers. These findings are consistent with the *in vitro* Western blot results and further support that PRXL2B regulates the PI3K/AKT pathway and PD-L1 expression *in vivo* (Figure 5k).

4. Discussion

This study identifies PRXL2B as a potential regulator of hepatocellular carcinoma progression and the antitumor efficacy of oncolytic adenovirus H101. Using integrated transcriptomic and proteomic analyses, we found that PRXL2B was consistently downregulated after H101 treatment in the murine tumor model, suggesting that it may be involved in the tumor response to oncolytic virotherapy. Functional assays further demonstrated that PRXL2B knockdown inhibited HCC cell proliferation,

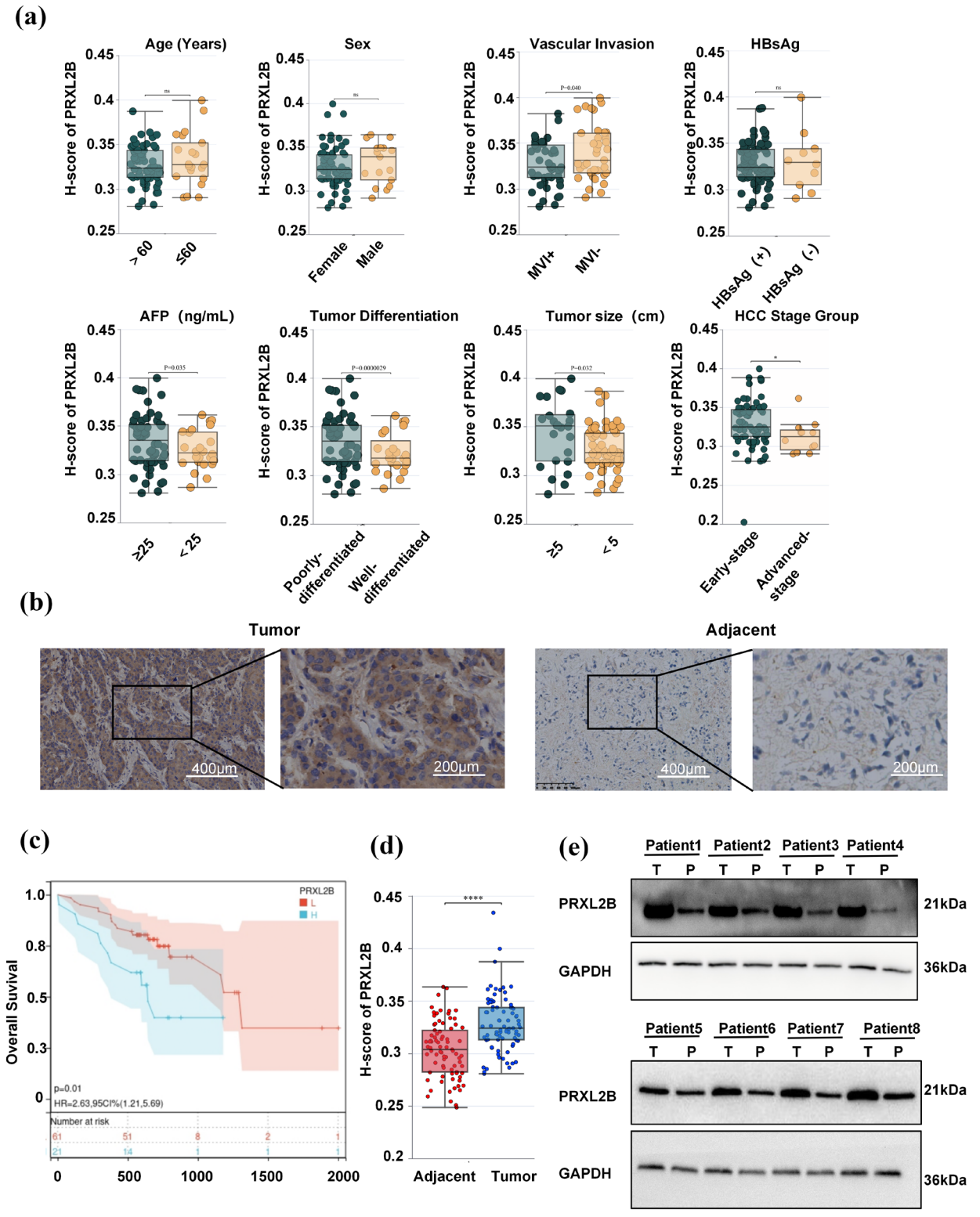

Figure 3. Clinical validation of PRXL2B expression in HCC tissue microarrays and its association with clinicopathological features and prognosis. (a) Correlation analysis between PRXL2B immunohistochemical staining (H-score) and clinicopathological characteristics in the HCC tissue microarray cohort (n = 84). **(b)** Representative immunohistochemical staining images of PRXL2B expression in tumor and paired adjacent tissues. Scale bars are indicated. **(c)** Kaplan–Meier overall survival analysis of PRXL2B expression in the LIHC cohort. **(d)** Comparison of PRXL2B H-scores between tumor and paired adjacent tissues. **(e)** Western blot analysis of PRXL2B protein expression in paired tumor **(T)** and adjacent **(P)** tissues, with GAPDH as a loading control.

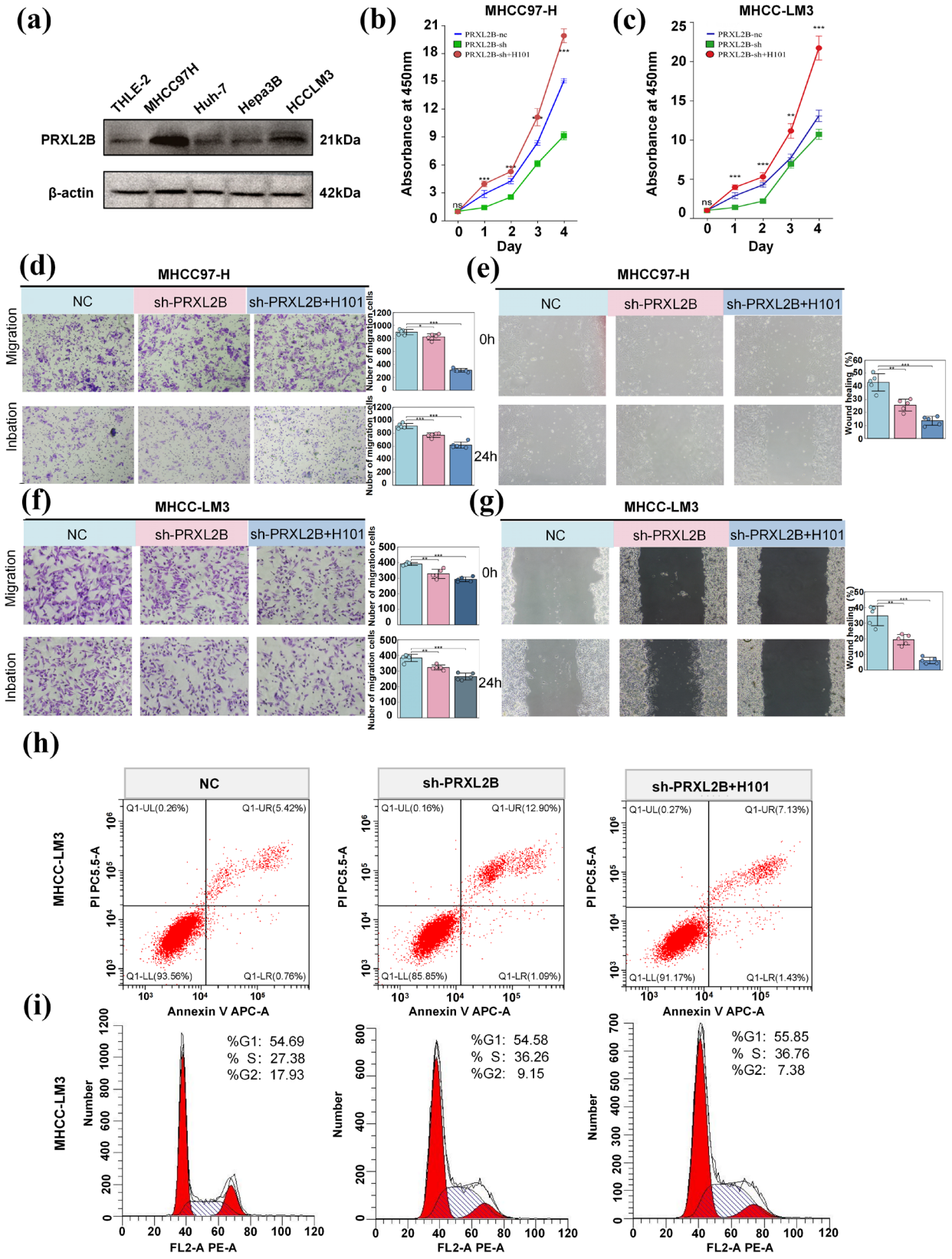

Figure 4. PRXL2B knockdown suppresses malignant phenotypes of HCC cells and enhances the effects of H101 *in vitro*. **(a)** Western blot analysis of PRXL2B expression in liver cancer cell lines, with GAPDH as a loading control. **(b–c)** CCK-8 assays of cell viability in MHCC97H **(b)** and HCCLM3 **(c)** cells under NC, shPRXL2B, and shPRXL2B + H101 conditions. Cells were infected with H101 (MOI = 0.05) for 96 h. **(d)** Transwell migration and invasion assays in MHCC97H cells. **(e)** Wound healing assays in MHCC97H cells at 0 h and 24 h, with quantification of wound closure. **(f)** Transwell migration and invasion assays in HCCLM3 cells. **(g)** Wound healing assays in HCCLM3 cells at 0 h and 24 h, with quantification of wound closure. **(h)** Flow cytometric analysis of apoptosis in HCCLM3 cells using Annexin V/PI staining. **(i)** Cell cycle distribution analysis of HCCLM3 cells using PI staining. Data are presented as mean ± SD. Statistical significance was determined using one-way ANOVA with post hoc testing.

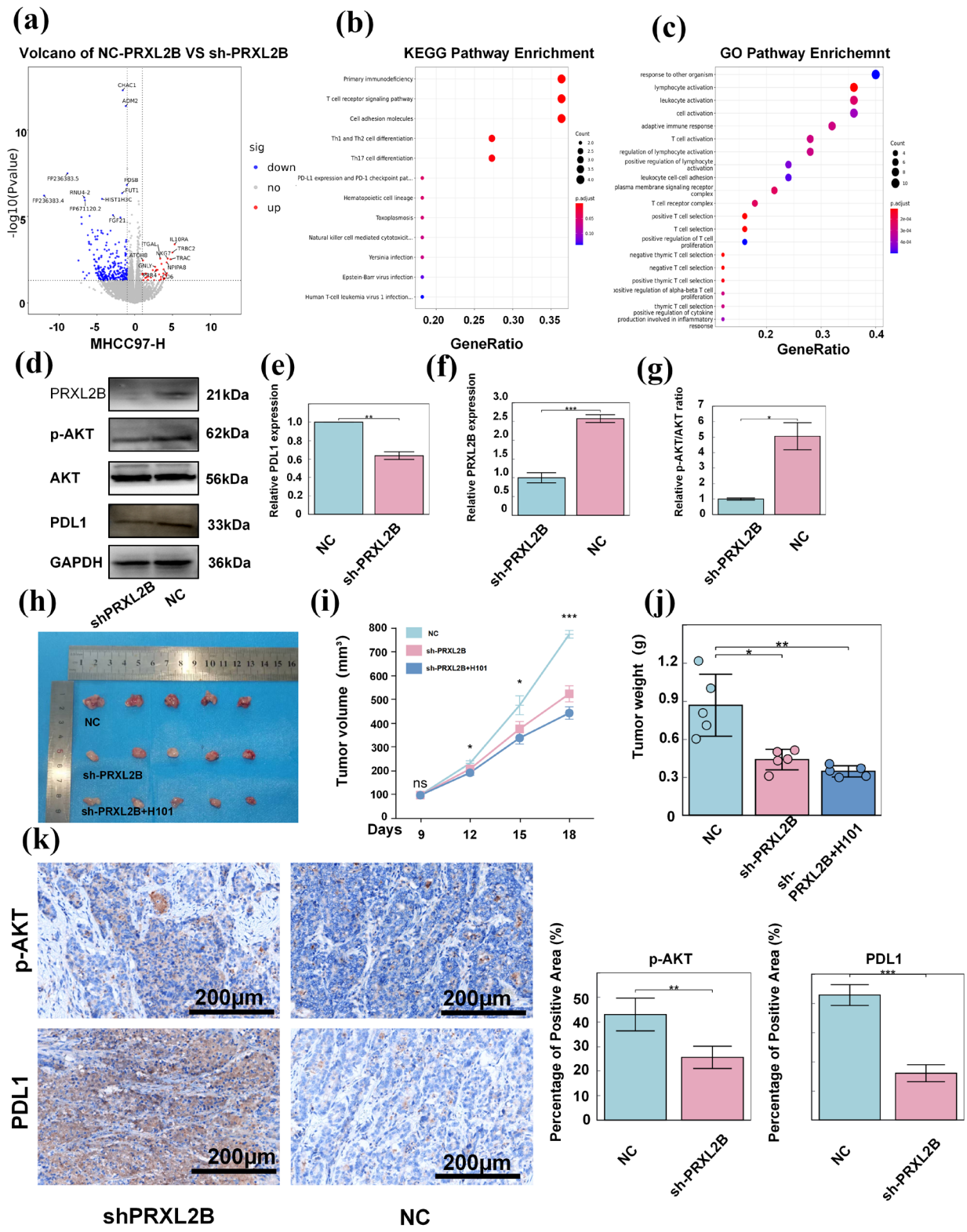

Figure 5. PRXL2B knockdown suppresses AKT signaling and PD-L1 expression and enhances the antitumor activity of H101. (a) Volcano plot of DEGs identified by RNA-seq analysis in NC and shPRXL2B MHCC97H cells. **(b)** KEGG pathway enrichment analysis of DEGs following PRXL2B knockdown. The x-axis indicates GeneRatio. Dot size represents gene counts, and dot color indicates adjusted *p* values. **(c)** GO enrichment analysis of DEGs following PRXL2B knockdown. **(d)** Representative Western blots of PRXL2B, PD-L1, p-AKT, total AKT, and GAPDH in MHCC97H cells under NC, shPRXL2B, and shPRXL2B + H101 conditions. Cells were infected with H101 (MOI = 0.05) for 96 h. **(e–g)** Densitometric quantification of PD-L1, PRXL2B, and p-AKT/AKT levels. **(h)** Representative images of excised tumors from Hepa1-6 subcutaneous tumor models in the NC, shPRXL2B, and shPRXL2B + H101 groups. Solid line = NC (negative control) and dashed line = shPRXL2B (PRXL2B knockdown). **(i–j)** Tumor growth curves **(i)** and tumor weights at the experimental endpoint **(j)**. Data are presented as mean ± SD with individual values. Statistical significance was determined using one-way ANOVA with post hoc testing. **(k)** Representative immunohistochemical staining images of p-AKT and PD-L1 in tumor tissues, with quantification shown on the right. Data are presented as mean ± SD.

migration, and invasion, promoted apoptosis, and enhanced the antitumor effect of H101 both *in vitro* and *in vivo*. These findings support a tumor-promoting role of PRXL2B in HCC and suggest that PRXL2B may represent a promising target for combination therapy with oncolytic viruses.

In addition to PRXL2B-mediated effects, our study highlights the therapeutic potential of H101 as an oncolytic adenovirus in HCC. Oncolytic viruses selectively replicate in tumor cells and induce tumor lysis while stimulating antitumor immunity (*18*). H101 treatment alone can trigger immunogenic cell death, recruit immune effector cells, and enhance tumor antigen presentation, which may synergize with immune checkpoint modulation (*19*). The observed downregulation of PRXL2B after H101 treatment suggests that viral replication and the host response may directly or indirectly modulate oncogenic signaling pathways (*20*). These findings imply that combining H101 with molecularly targeted interventions, such as PRXL2B inhibition, could enhance tumor cell killing and overcome intrinsic resistance mechanisms (*21*). Future studies should further investigate the impact of H101 on the tumor microenvironment, including innate and adaptive immune responses, and explore combination strategies with immune checkpoint inhibitors to improve therapeutic efficacy in HCC.

Our tissue-based validation and public dataset analyses consistently showed that PRXL2B was upregulated in HCC tissues. This finding is in line with a potential oncogenic role of PRXL2B in liver cancer. However, although PRXL2B expression was elevated in tumors, its associations with clinicopathological features and survival were not consistently significant in our tissue microarray cohort. This discrepancy between public dataset-based analyses and our clinical validation cohort may be attributed to differences in sample size, patient heterogeneity, cutoff selection, and follow-up duration (*22*). Therefore, while PRXL2B appears to be involved in HCC progression, its value as an independent prognostic biomarker remains inconclusive and requires further validation in larger and well-characterized clinical cohorts.

Mechanistically, our data suggest that PRXL2B may exert its effects through the PI3K/AKT/PD-L1 axis. PRXL2B knockdown reduced p-AKT and PD-L1 expression in HCC cells, indicating that PRXL2B may contribute not only to tumor cell survival but also to immune evasion. Because the PI3K/AKT pathway plays a central role in tumor growth, survival, and therapeutic resistance, its suppression after PRXL2B silencing provides a plausible mechanistic basis for the observed antitumor effects (*23*). In addition, the reduction in PD-L1 expression suggests that PRXL2B may influence the immunosuppressive phenotype of HCC, thereby affecting responsiveness to oncolytic virus therapy. To further support the *in vivo* relevance of this mechanism, we supplemented immunohistochemical staining of tumor tissues from the animal experiments. The results showed that p-AKT and PD-L1 expression were decreased in the shPRXL2B group compared with the NC group, and were further reduced in the combination treatment group, which was consistent with our Western blot findings. These data strengthen the evidence that PRXL2B regulates the PI3K/AKT/PD-L1 axis *in vivo* and further support its involvement in tumor progression and therapeutic response (*24*).

The combination of PRXL2B knockdown and H101 produced the strongest antitumor effect *in vivo*, suggesting that PRXL2B inhibition may enhance the efficacy of oncolytic virotherapy (*25*). This combinational strategy warrants further investigation. Nevertheless, several limitations of this study should be acknowledged. First, although PRXL2B was upregulated in HCC, its clinical significance was not consistently confirmed in our tissue microarray cohort. Second, an H101-alone treatment group was not included in the current study, which limits our ability to fully distinguish the independent effect of H101 from its interaction with PRXL2B knockdown. Third, although our data support the involvement of the PI3K/AKT/PD-L1 axis, other signaling pathways, such as NF-kB or JAK/STAT, may also participate in PRXL2B-mediated regulation and deserve further study (*26*). Overall, our findings indicate that PRXL2B contributes to HCC malignant progression and may modulate the therapeutic response to H101. Future studies should focus on validating PRXL2B in larger clinical cohorts, clarifying its predictive value for oncolytic virus therapy, and exploring whether PRXL2B-targeted interventions can improve the efficacy of combination treatment strategies in HCC.

Funding: This work was supported by the National Natural Science Foundation of China (No. 82170666 and 82572988), the First-Class Discipline-Mentoring Team (No. 030102050401CYYY-DSTDXM-202411), and the Key Project of Nutrition and Health Special Fund of Chongqing Maternal and Child Health Association Research Fund Management Committee (No. CQMCHA-NH2025-03).

Conflict of Interest: The authors have no conflicts of interest to disclose.

Data Availability: The RNA-seq and proteomics datasets generated and/or analyzed during the current study are available from the corresponding author upon reasonable request. The clinical information from the tissue microarray cohort contains sensitive patient-related data and is therefore available only upon reasonable request and with appropriate ethical approval. All other data supporting the findings of this study are included in the manuscript and Supplementary Information.

References

1. Anwanwan D, Singh SK, Singh S, Saikam V, Singh R. Challenges in liver cancer and possible treatment approaches. Biochim Biophys Acta Rev Cancer. 2020; 1873:188314.
2. Raja J, Ludwig JM, Gettinger SN, Schalper KA, Kim HS. Oncolytic virus immunotherapy: future prospects for oncology. J Immunother Cancer. 2018; 6:140.
3. Abudoureyimu M, Lai Y, Tian C, Wang T, Wang R, Chu X. Corrigendum: Oncolytic Adenovirus-A Nova for Gene-Targeted Oncolytic Viral Therapy in HCC. Front Oncol. 2020; 10:701.
4. Mantwill K, Klein FG, Wang D, Hindupur SV, Ehrenfeld M, Holm PS, Nawroth R. Concepts in Oncolytic Adenovirus Therapy. Int J Mol Sci. 2021; 22:10522.
5. Duan Y, Bai H, Li X, Wang D, Wang Y, Cao M, Zhang N, Chen H, Wang Y. Oncolytic Adenovirus H101 Synergizes with Radiation in Cervical Cancer Cells. Curr Cancer Drug Targets. 2021; 21:619-630.
6. Qiao C, Xu Y, He Y, Cai Z, Wang H. Oncolytic adenovirus H101 enhances the anti-tumor effects of PD-1 blockade *via* CD47 downregulation in tumor cells. Oncol Res. 2025; 33:1161-1172.
7. Xi P, Zeng D, Chen M, Jiang L, Zhang Y, Qin D, Yao Z, He C. Enhancing pancreatic cancer treatment: The role of H101 oncolytic virus in irreversible electroporation. Front Immunol. 2025; 16:1546242.
8. Santos Apolonio J, Lima de Souza Gonçalves V, Cordeiro Santos ML, Silva Luz M, Silva Souza JV, Rocha Pinheiro SL, de Souza WR, Sande Loureiro M, de Melo FF. Oncolytic virus therapy in cancer: A current review. World J Virol. 2021; 10:229-255.
9. Kaufman HL, Kohlhapp FJ, Zloza A. Oncolytic viruses: a new class of immunotherapy drugs. Nat Rev Drug Discov. 2015; 14:642-662.
10. van Lieshout L, van de Stolpe A, van der Ploeg P, Bowtell D, de Hullu J, Piek J. Signal Transduction Pathway Activity in High-Grade, Serous Ovarian Carcinoma Reveals a More Favorable Prognosis in Tumors with Low PI3K and High NF-κB Pathway Activity: A Novel Approach to a Long-Standing Enigma. Cancers (Basel). 2020; 12:2660.
11. Song D, Jia X, Liu X, *et al*. Identification of the receptor of oncolytic virus M1 as a therapeutic predictor for multiple solid tumors. Signal Transduct Target Ther. 2022; 7:100.
12. Shi ZR, Duan YX, Cui F, Wu ZJ, Li MP, Song PP, Peng QL, Ye WT, Yin KL, Kang MQ, Yu YX, Yang J, Tang W, Liao R. Integrated proteogenomic characterization reveals an imbalanced hepatocellular carcinoma microenvironment after incomplete radiofrequency ablation. J Exp Clin Cancer Res. 2023; 42:133.
13. Cheng AL, Hsu C, Chan SL, Choo SP, Kudo M. Challenges of combination therapy with immune checkpoint inhibitors for hepatocellular carcinoma. J Hepatol. 2020; 72:307-319.
14. Budhu A, Roessler S, Zhao X, Yu Z, Forgues M, Ji J, Karoly E, Qin LX, Ye QH, Jia HL, Fan J, Sun HC, Tang ZY, Wang XW. Integrated metabolite and gene expression profiles identify lipid biomarkers associated with progression of hepatocellular carcinoma and patient outcomes. Gastroenterology. 2013; 144:1066-1075. e1061.
15. Amicone L, Citarella F, Cicchini C. Epigenetic regulation in hepatocellular carcinoma requires long noncoding RNAs. Biomed Res Int. 2015; 2015:473942.
16. Gao Q, Zhu H, Dong L, *et al*. Integrated Proteogenomic Characterization of HBV-Related Hepatocellular Carcinoma. Cell. 2019; 179:561-577.e522.
17. Song W, Yuan Y, Cao F, Pan H, Liu Y. The key pathways and genes related to oncolytic Newcastle disease virus-induced phenotypic changes in ovarian cancer cells. J Microbiol. 2025; 63:e2411018.
18. Marchini A, Ilkow CS, Melcher A. Oncolytic Virus Immunotherapy. Cancers (Basel). 2021; 13:3672.
19. Ghasemi Darestani N, Gilmanova AI, Al-Gazally ME, Zekiy AO, Ansari MJ, Zabibah RS, Jawad MA, Al-Shalah SAJ, Rizaev JA, Alnassar YS, Mohammed NM, Mustafa YF, Darvishi M, Akhavan-Sigari R. Mesenchymal stem cell-released oncolytic virus: an innovative strategy for cancer treatment. Cell Commun Signal. 2023; 21:43.
20. Kaufman HL, Maciorowski D. Advancing oncolytic virus therapy by understanding the biology. Nat Rev Clin Oncol. 2021; 18:197-198.
21. Wang Z, Sun P, Li Z, Xiao S. Clinical Advances and Future Directions of Oncolytic Virotherapy for Head and Neck Cancer. Cancers (Basel). 2023; 15:5291.
22. Kui X, Wang Y, Zhang C, Li H, Li Q, Ke Y, Wang L. Prognostic value of SH3PXD2B (Tks4) in human hepatocellular carcinoma: a combined multi-omics and experimental study. BMC Med Genomics. 2021; 14:115.
23. He Y, Sun MM, Zhang GG, Yang J, Chen KS, Xu WW, Li B. Targeting PI3K/Akt signal transduction for cancer therapy. Signal Transduct Target Ther. 2021; 6:425.
24. Nishida N, Sakai K, Morita M, Aoki T, Takita M, Hagiwara S, Komeda Y, Takenaka M, Minami Y, Ida H, Ueshima K, Nishio K, Kudo M. Association between Genetic and Immunological Background of Hepatocellular Carcinoma and Expression of Programmed Cell Death-1. Liver Cancer. 2020; 9:426-439.
25. Samson A, Bentham MJ, Scott K, *et al*. Oncolytic reovirus as a combined antiviral and anti-tumour agent for the treatment of liver cancer. Gut. 2018; 67:562-573.
26. Hin Tang JJ, Hao Thng DK, Lim JJ, Toh TB. JAK/STAT signaling in hepatocellular carcinoma. Hepat Oncol. 2020; 7:HEP18.

Received January 5, 2026; Revised May 2, 2026; Accepted May 18, 2026.

[§]These authors contributed equally to this work.
**Address correspondence to:*
Ping Che, Department of Hepatobiliary Surgery, Shapingba Hospital affiliated to Chongqing University (Shapingba District People's Hospital of Chongqing), No. 2, Jialang Road, Shapingba District, Chongqing 400030, China.
E-mail: dr.che@cqu.edu.cn

Rui Liao, Department of Hepatobiliary Surgery, The First Affiliated Hospital, Chongqing Medical University, No.1, Youyi Road, Yuzhong District, Chongqing 400016, China.
E-mail: liaorui99@163.com

Released online in J-STAGE as advance publication May 21, 2026.